Heliyon 10 (2024) e33117

Contents lists available at ScienceDirect

Heliyon

journal homepage: www.cell.com/heliyon

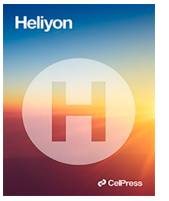

Research article

The effect of $ZnSO_4$ and $Fe_2(SO_4)_3$ on the pyrolysis of cocoa shells: A tg-FTIR study

Angie Xiomara Vesga, María Fernanda Cuentas, Alberto Ricardo Albis Arrieta *

Faculty of Engineering, Program of Chemical Engineering, Universidad del Atlántico, Carrera 30 8-49, 80001, Puerto Colombia, Atlántico, Colombia

ARTICLE INFO

Keywords:
Thermogravimetric analysis
Infrared spectroscopy
Kinetics
Distributed activation energy model

ABSTRACT

Pyrolysis stands out as one potential route for valorizing abundant agro-industrial cocoa residues. However, the products of this reaction, particularly bio-oil, do not possess the required quality for direct use in many applications. Thus, this study explores the use of iron sulfate and zinc sulfate as potential catalysts in the pyrolysis of these residues. In this investigation, the biomass, previously ground and dried, was impregnated with varying percentages of ferric sulfate and zinc sulfate. The TG-FTIR technique was employed to ascertain the effect of these salts on the pyrolysis of cocoa shell. The results were fitted with the DAEM model with three pseudo-components. It was determined that both salts induced alterations in the DTG profiles of the thermal decomposition of cocoa shell. In the evolved gases, compounds such as CO_2, H_2O, CH_4, CO, HCN, and oxygenated compounds like HCOOH and CH_3COOH were detected. Ferric sulfate significantly influenced the activation energies governing the reactions of the three pseudo-components. Conversely, the presence of zinc sulfate did not alter the activation energies associated with the decomposition of cocoa shell pseudo-components. Both catalysts induced alterations in the infrared spectra of the evolved gases, which is primarily evident in the relative intensities of bands corresponding to the stretching vibrations of constituent groups within CO_2, CO, water, and oxygenated compounds.

1. Introduction

Biomass is currently considered an important renewable resource that can contribute to a country's economy, sustainability, and energy security [1]. One of the main advantages of using biomass for energy and power generation is that it is a cleaner source of energy than fossil fuels, due to its low nitrogen, sulfur, and ash content, which minimizes emissions of sulfur dioxide (SO_2) and nitrogen oxides (NOx) [2].

Cocoa shells are often regarded as waste from cocoa production, and thus, several applications have been proposed for their use. These include utilization as farm animal feed, a precursor for potassium salts and soap production, and energy recovery through thermal processes such as pyrolysis, gasification, and bioethanol production [3].

Among the technologies proposed for energy recovery, pyrolysis stands out due to the possibility of producing liquid fuels such as bio-oil and solid products with several potential applications [4]. However, several studies of pyrolysis of different types of biomasses have shown that the bio-oil obtained does not meet the quality standards for direct use in internal combustion engines. Therefore, subjecting the bio-oil to further upgrading processes is necessary, which considerably increases production costs. Catalytic pyrolysis is a method that can potentially improve the quality of the bio-oil and, in turn, reduce production costs if the appropriate catalysts are

* Corresponding author.
E-mail address: albertoalbis@uniatlantico.edu.co (A.R. Albis Arrieta).

https://doi.org/10.1016/j.heliyon.2024.e33117
Received 21 October 2023; Received in revised form 4 June 2024; Accepted 14 June 2024
Available online 20 June 2024

used [5].

The catalytic pyrolysis of metal-impregnated biomass has garnered significant attention, highlighting the need for a comprehensive understanding of the influence of heavy metals as catalysts on pyrolysis products [6]. Interactions between biomass and alkali minerals, alkaline earth minerals, and metallic salts, such as zinc and nickel chlorides, have been extensively studied, as well as the impact of iron and copper salts in wood pyrolysis and iron in rapid pyrolysis of biomass and cellulose mixtures. These catalysts are expected to facilitate the cleavage of pyranose rings in biomass polysaccharides and the depolymerization of lignin. Furthermore, investigations into heavy metals, metal combinations, metallic salts, oxides, acidic oxides, zeolites, and organic and inorganic salts, have provided valuable insights [6–12]. Notably, calcium oxide-based catalysts have shown promise in reducing tar during gasification, and the utilization of Ni-based catalysts supported on dolomite has increased H_2 production during pyrolysis/gasification of $ZnCl_2$-impregnated biomass [13–15]. Additionally, the effect of metallic salts as catalysts in biomass pyrolysis has been studied in detail by various researchers. The study by Chen et al. involved the analysis of biomass pyrolysis phenomena and mechanisms using Zeolite Socony Mobil-5 (ZSM-5) as a catalyst, where the optimum biomass-to-catalyst ratio of 1/10 led to intensified aromatic hydrocarbons (AHs) formation, especially for sawdust [16]. These findings underscore the importance of understanding the role of heavy metals as catalysts in pyrolysis processes to advance sustainable biofuel production and chemical valorization of biomass [17].

The electronic properties of transition metals such as Fe and Zn are expected to play a pivotal role in the thermal decomposition processes of biomass, as explored by several authors. The pyrolysis of empty palm oil fruit catalyzed by zinc sulfate supported on ZSM-5 zeolite exhibited an increase in bio-oil yield [18]. In the pyrolysis of corn biomass, it was found that zinc sulfate reduces hemicellulose fragmentation, promotes cellulose degradation, and enhances the repolymerization process of primary degradation products [19]. The study on the use of residues with high sulfur and zinc content as catalysts demonstrated that ZnSOx-centered super strong acid sites are Brønsted acids that significantly enhance the extent of deoxygenation of biomass [20]. In contrast, another study demonstrated that zinc sulfate had no effect on Willow pyrolysis. However, the pyrolysis process using zinc sulfate and zinc nitrate showed that sample preparation changed the matrix and the biomass physical-chemical properties, increasing the thermal stability of cellulose during pyrolysis [21]. Thus, biomass pyrolysis in the presence or absence of zinc catalysts must be prepared carefully to gain reliable and comparable results [22].

On the other hand, it was reported that ferrous sulfate alters the product distribution in the pyrolysis of cottonwood and newspaper, lowers the pyrolysis temperature, and increases the production of levoglucosan and levoglucosanone [23], and sugars in the pyrolysis of corn stover. Similar results were obtained for cellulose and pine wood using ferric sulfate [12]. Hydrolysis of these compounds can generate glucose and be used to synthesize chiral polymers such as glucan [24]. Similarly, it has been found that both ferric sulfate and zinc sulfate change the thermogram profile of lignin [25]. The pyrolysis of waste biomass and hydrocarbonized materials impregnated with iron (Fe) demonstrated that this metal enhances the degree of carbonization, resulting in lower H/C ratios [26]. Other studies have included Ru/Fe-impregnated banana pseudo-stem [9], and copper and iron salts as additives in wood pyrolysis [27]. Ferrous sulfate has been identified as a promising pretreatment of corn stover for autothermal pyrolysis in fluidized bed reactors achieving volumetric sugar productivities 32 times higher than conventional pyrolysis [14]. Considering the aforementioned results, further studies are necessary to ascertain the role of Fe and Zn in the pyrolysis of various types of biomasses.

Thermoanalytical techniques, notably thermogravimetric analysis (TG) and derivative thermogravimetry (DTG), serve as pivotal tools for probing the pyrolytic and kinetic solid materials attributes [28]. Amidst the array of kinetic models employed for thermogravimetric data fitting, the distributed activation energy model (DAEM) stands out for its capacity to facilitate the interpretation of outcomes in the context of biomass macro-components [29,30]. The influence of factors such as biomass composition, process parameters, and catalyst types, among others, on the prevalent reactions in pyrolysis is noteworthy, as they directly affect product composition, properties, and yields [31–33]. Evolved gas analysis is a tool that would give insights on the potential effect of catalysts on the pyrolysis of various types of biomasses.

The DAEM has been used in fitting the pyrolysis of various biomasses. For instance Ref. [34], successfully used a double Gaussian DAEM to properly describe the pyrolysis of algae biomass and sub-bituminous coal. Furthermore, while the modeling of pyrolysis of woody biomass utilized three pseudo-components, four were employed for herbaceous materials [35]. Generally, in most cases, three sets of parallel reactions are used to model biomass pyrolysis [36]. DAEM performance has also been compared with other models: a comparison of several methods with DAEM and the development of a new fitting hybrid approach was tested in the pyrolysis of duckweed: the hybrid approach with parallel reactions (including DAEM with three sets of reactions) showed superior performance than the conventional DAEM and iso-conversional methods [37]. The DAEM equations are complex and the estimation of DAEM parameters has mathematical difficulties reflected in several fitting procedures reported in the literature. This includes distribution-free and distribution-fitting methods, and differential and integral methods [36]. As the number of sets of parallel reactions increases, so does the number of parameters. In some cases, it becomes necessary to fix some parameters, such as the pre-exponential factors of each reaction set, using literature-derived data. Optimization routines include direct search methods [38,39], and nonlinear optimization (e.g. nonlinear Hooke and Jeeves optimizing method, Marquardt nonlinear regression method) [40–42].

In this study, the DAEM model was used to evaluate the devolatilization kinetics of cocoa shell residues, both with and without the presence of ferric sulfate and zinc sulfate, using the TG-FTIR technique. This allowed for the determination of biochar yields and an evaluation of the influence of catalysts on the kinetic parameters governing the pyrolysis of the biomass macro-components. Furthermore, the study successfully identified specific compound groups within the evolved gases and analyzed their temporal evolution profile relative to temperature. These measurements facilitated an assessment of the catalytic effect exerted by zinc sulfate and ferric sulfate in the pyrolysis of cocoa shell residues.

2. Materials and methods

2.1. Materials

Iron (III) sulfate ($Fe_2(SO4)_3{\cdot}XH_2O$) (75 %), and zinc sulfate ($ZnSO_4{\cdot}7H_2O$) (99 %) were purchased from sigma. Cocoa shell residue was collected from a cocoa farm in the San Vicente de Chucurí Municipality, located in Santander-Colombia.

2.2. Biomass characterization

The proximate and ultimate analyses were determined according to the following standards: calorific value (ASTM D-5865-13), moisture (ASTM D-3173-17), ash (ASTM D-3174-12), volatile material (ASTM D-3175-17), fixed carbon (by difference), sulfur (ASTM D-4239-17 Method A), and elemental analysis (C, H, N, O; ASTM D-5373-16) (Table 1).

2.3. Biomass preparation

The cocoa shell was dried at 80 °C to constant weight, milled, sieved to a particle size of around 70 μm, and stored for later use. The catalysts, zinc sulfate heptahydrate ($ZnSO_4 \bullet 7H_2O$) and ferric sulfate X-hydrate $Fe_2(SO_4)_3$, were oven-dried at 105 °C and 200 °C, respectively. Next, 4 suspensions of 1.000 g of cocoa shells were prepared with 14.0 mL of distilled water, and appropriate amounts of catalyst to obtain catalyst concentrations of 1.5 and 3.0 % w/w (dried biomass basis). The suspensions were stirred at 70 rpm for 2 h and dried at 105 °C, for 2 h. Subsequently, they were collected and reserved in the desiccator until further use. All samples were prepared and analyzed in triplicate.

2.4. Thermogravimetric analysis coupled with Fourier transform infrared spectroscopy (TGA/FTIR)

FTIR analysis has been successfully used to identify functional groups. Combining this technique with TGA analysis allows a complete characterization of the materials regarding thermal stability and decomposition mechanisms, forming a complete integrated system for TGA/FTIR analysis [43]. Combining both techniques provides a complete sample analysis with quantitative TGA weight loss data and identification of gases released by FTIR. These analyses were carried out on a SETSYS - 1750 CS EVO thermogravimetric balance (Setaram) coupled to an IRAffinity-1 FTIR (Shimadzu), in which nitrogen gas (purity grade 5) was used as a purge gas with a constant flow rate of 30 mL/min. For FTIR, a 10 cm path-length cell (PIKE) with KBr windows heated to 200 °C was used to analyze the evolved gases. The two instruments were connected by a line maintained at 200 °C to avoid condensation of the pyrolysis products. The TGA/FTIR experiments conducted on both biomass without catalysts and biomass impregnated with catalysts allowed determining the temperature ranges in which the cocoa shell degrades and the catalysts' impact on decomposition kinetic parameters.

Three heating ramps (5, 10, and 30 K/min) were used in a temperature range from 25 °C to 800 °C. The mass of the sample placed in the thermobalance was in the range of 11–13 mg. The DAEM model was adjusted to the experimental results of the pyrolysis process of cocoa shell residues in the presence and absence of catalysts. This model was used to determine the kinetic parameters of cocoa shell decomposition and product formation [30,44].

2.5. Experimental design

A factorial design with three variables (2 × 3 × 3) was used with repetitions at the central point: catalyst, catalyst percentage (0 %, 1.5 %, and 3 %), and heating ramp (5, 10, and 30 K/min); thus, obtaining a design of 21 experiments. The experiments were randomized, and multiple replications were performed for the tests with 1.5 % catalyst at the 10 K/min ramp.

Table 1
Proximate and ultimate analysis of cocoa shell.

Proximate analysis	% Mass (dry basis)
Moisture	9.76
Ash	10.57
Volatile matter	78.75
Fixed carbon[a]	10.68
Sulfur	0.19
Gross heating value, BTU/Lb	7206
Ultimate analysis	**% Mass**
Carbon	45.90
Hydrogen	5.26
Nitrogen	1.54
Oxygen[a]	36.54

[a] Calculated by difference.

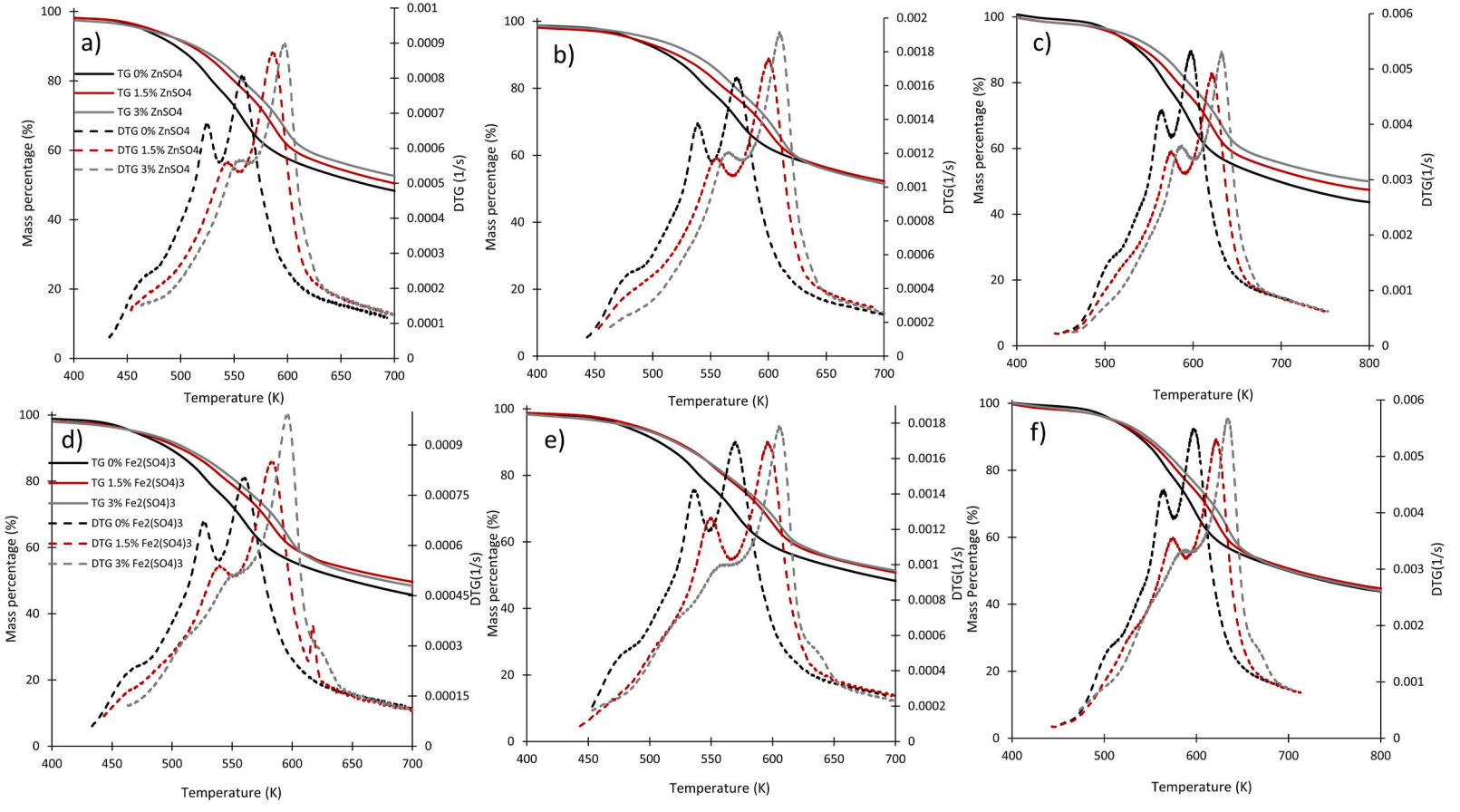

Fig. 1. TG and DTG thermograms of the pyrolysis of cocoa shells impregned with $ZnSO_4$ at several heating rates: a) 5 K/min, b) 10 K/min, c) 30 K/min; $Fe_2(SO_4)_3$: d) 5 K/min, e) 10 K/min, f) 30 K/min.

2.6. Distributed activation energy model (DAEM)

The distributed activation energy model (DAEM) is a parallel reaction model where a Gaussian distribution for the activation energies is assumed [30]. According to this model, the thermal degradation of the material occurs in a superposition of multiple parallel steps. Each step in the reaction is assumed to be composed of an infinite number of parallel reactions occurring simultaneously, having different values of activation energies and frequency factors [45].

In this model, the sample is considered a combination of M pseudo-components. A pseudo-component is the totality of decomposed species that can be described by the same reaction kinetic parameters in the model. The number of reacting species is larger in complex mixtures. The differences in reactivity are described by the different activation energy values. On a molecular level, each pseudo-component j is assumed to undergo a first-order decay. The rate constant k is assumed to be temperature-dependent according to the Arrhenius equation [30]. A scheme consisting of three independent first-order reactions, or three pseudo-components was used in this study.

The first derivative of the thermogravimetric curve (DTG) is fitted with equation (1):

$$Y^{calc}(t) = -\sum_{j=1}^{M} c_j \frac{dx_j}{dt} \tag{1}$$

where x_j is the fraction of unreacted material represented by the kinetic equation of order j and c_j indicates the contribution of the j-th equation to the measured quantity. On the other hand, M corresponds to the number of pseudo-components or sets of reactions that can be described through the same distribution function. The activation energies for the reactions involved are considered to be distributed in a Gaussian distribution function with parameters E_{0j} and σ_j. If the solution of a first-order kinetic equation at a given value of E is denoted as $X_j(t,E)$, the x_j functions of equation (1) can be calculated by means of equation (2) [30,46].

$$x_j(t) = \int_{-\infty}^{\infty} \frac{1}{\sqrt{2\pi}\,\sigma}\, exp\left[-\frac{\left(E - E_{0j}\right)^2}{2\sigma^2}\right] X_j(t,E)dE \tag{2}$$

3. Results and discusión

3.1. Biomass characterization

Table 1 displays the proximate and ultimate analysis outcomes of cocoa shell residues, which align closely with previously documented findings in the literature related to this biomass type [47]. The ash content of the sample registers at 10.57 %, a value in close correspondence to the 10.5 % reported by Ref. [48]. The volatile matter content of 78.75 % bears similarity to the figures delineated by Ref. [47], specifically 71.81 %. It is also comparable to the value of 76.4 % as reported by Ref. [49]. Conversely [48], observed a lower volatile matter content of 66.6 %. As for fixed carbon, the obtained result of 10.68 % closely aligns with the figures reported by Refs. [47,49], which are 9.48 % and 11.6 %, respectively. It is worth noting, however, that other researchers have reported higher fixed carbon values for this same biomass. For instance Refs. [48,50], obtained results of 22.9 % and 23.8 %, respectively.

3.2. Thermogravimetric analysis

The thermogravimetric (TG) curves generated during the pyrolysis process of cocoa shells were subjected to detailed analysis, considering experiments conducted under varying heating rates of 5, 10, and 30 K/min. The initial dry mass was determined at 394 K, and the pyrolysis event was delineated to occur within the temperature range of 473 K–923 K. Notably, the DTG thermogram for the cocoa shell sample in the absence of catalyst, as depicted in Fig. 1, facilitated the discernment of three distinct pyrolysis phases, likely corresponding to the thermal breakdown of extractable compounds and the lignocellulosic macro-components, namely hemicellulose and cellulose.

In Fig. 1, the most substantial mass loss is observed within the temperature interval of 500–600 K. As expected, within this same range, the maximal rates of mass loss, denoted by peaks in the DTG, are recorded. The initial pyrolysis stage transpires between 450 and 580 K, aligning with the onset of the initial event attributed to hemicellulose pyrolysis. According to existing literature, this phase typically occurs between 483 and 598 K [51]. A subsequent peak, characterized by an elevated decomposition rate, manifests between 530 and 650 K, which indicates of cellulose pyrolysis. The literature commonly reports the maximum mass loss for cellulose to fall within the range of 550–650 K. Finally, lignin pyrolysis is documented to occur within the temperature span of 433–750 K, featuring notably low mass loss rates with maxima around 650 K [22,44,52,53].

Published studies present varying compositional analyses of cocoa shell's lignocellulosic constituents [47]. reports a composition of 44.39 % lignin, 52.43 % holocellulose, and 10.4 % ash. Conversely [49], document results of 37.2 % lignin, 38.2 % holocellulose (19.6 % cellulose and 18.6 % hemicellulose), and 24.5 % ash. These findings corroborate the results obtained in this study, implying that this biomass possesses potential for assessment in biofuel production through thermo-conversion. Moreover, an anticipated overlap in the pyrolysis of the three macro-components suggests a devolatilization mechanism characterized by multiple parallel reactions [34,35].

Fig. 1a-f demonstrates that as both the heating rate and the proportion of catalyst increase, regardless of the catalyst type, there is a corresponding rise in the temperature at which the peak mass loss rate occurs. In the absence of a catalyst, the recorded temperatures

are consistently lower compared to those observed in the presence of a catalyst under equivalent heating rates (5, 10, and 30 K/min), yielding respective values of 559.8 K, 569.5 K, and 597.9 K. In the context of cocoa shell pyrolysis employing a 1.5 % zinc sulfate catalyst, temperature peaks were discerned at 586.2 K, 600.4 K, and 620.5 K for heating rates of 5, 10, and 30 K/min, respectively. With a 3 % zinc sulfate addition, corresponding peaks were registered at temperatures of 597.1 K, 609.6 K, and 632.1 K, under the same heating rates. A comparable trend is observed in pyrolysis with a ferric sulfate catalyst: incorporating 1.5 % ferric sulfate catalyst at heating rates of 5, 10, and 30 K/min yielded temperature peaks of 583.5 K, 595.5 K, and 620.8 K, respectively. With a 3 % addition of the same catalyst, temperature peaks were recorded at 596.7 K, 605.6 K, and 634.3 K, again at heating rates of 5, 10, and 30 K/min, respectively.

Based on the observed temperatures of the mass loss peaks in the derivative thermogravimetric (DTG) profiles (Fig. 1), it is evident that hemicellulose and cellulose are the predominant constituents within cocoa shells. Furthermore, this figure illustrates that, for a constant catalyst concentration, the temperature corresponding to both peaks rises as the heating rate increases, aligning with anticipated behavior for a chemical reaction.

Likewise, in Fig. 7a, b, and 7c, it is apparent that elevating the concentration of zinc sulfate leads to a reduction in the maximum mass loss linked to hemicellulose decomposition, as well as a concurrent increase in associated temperature. This trend is more pronounced when employing ferric sulfate as a catalyst (Fig. 7d, e, and 7f). Consequently, augmenting the ferric sulfate concentration to 3 % results in the disappearance of the peak associated with hemicellulose decomposition, replaced by a shoulder across all studied heating rates. This suggests a substantial alteration in the cocoa shell pyrolysis mechanism induced by the presence of both salts. Analogous findings have been documented in the pyrolysis of other biomasses such as empty fruit bunches from oil palm [22] and African palm husk [52]. In contrast, in the pyrolysis of residues from the cassava starch industry, ferric sulfate exhibited a pronounced influence on lignin pyrolysis, while exerting negligible effects on cellulose and hemicellulose pyrolysis [54]. Moreover, both catalysts demonstrated an elevation in pyrolysis temperature and activation energy for lignin [25] and a reduction in hemicellulose pyrolysis temperature [24].

Table 2 presents the biochar yields and corresponding mass losses under varying heating rates and catalyst concentrations. Observably, zinc sulfate exhibits a slight detrimental impact on biochar yield when comparing experiments conducted at equivalent heating rates: an increase in catalyst concentration correlates with a reduction in biochar percentage. In stark contrast, ferric sulfate manifests an opposing trend; as its concentration escalates, the biochar percentage slightly rises, indicating an augmented yield of this product. Notably, Table 2 underscores minimal fluctuations in mass loss relative to both heating rate and catalyst concentration. The highest mass loss, reaching 71.17 %, was recorded in the experiment conducted at a heating rate of 5 K/min with 1.5 % ferric sulfate catalyst. Conversely, the lowest mass loss, measuring 65.98 %, was observed in the sample lacking catalyst at a heating rate of 10 K/min. In summary, it can be deduced that both catalysts only slightly influenced the ultimate biochar yield.

3.3. Kinetic modeling

The DAEM encapsulates the thermal degradation of biomass through an ensemble of concurrent reactions, characterized by identical frequency factor values, and normally distributed activation energy values. These activation energies are defined by an average value and a standard deviation. Due to the lack of an analytical solution for Equations (1) and (2), numerical programming using Matlab® was employed for their resolution. In this study, three distinct sets of parallel reactions, denoted as pseudo-components, were employed, conventionally correlated with the principal constituents of biomass: hemicellulose, cellulose, and lignin [51,55]. Although a reduced number of pseudo-components were investigated, the resultant outcomes were deemed unsatisfactory (refer to supplementary material).

Table S1 provides the kinetic parameters derived from the DAEM model employing three pseudo-components, elucidating the pyrolysis of cocoa shell waste under distinct heating rates of 5, 10, and 30 K/min, both in the absence and presence of the two catalysts. These parameters were determined through the fitting of DTG data to the kinetic model [56]. The table encompasses key values,

Table 2
Percentage of mass loss, percentage of char and temperature of maximum mass loss, at several heating rates and percentages of catalyst.

	Heating rate (K/min)	Catalyst percentage (%)	Weight loss (%)	Char (%)	Peak temperature (K)
No catalyst	5	0	66.59	33.41	558.42
	10	0	65.98	34.02	571.1
	30	0	65.99	34.01	597.97
$ZnSO_4$	5	1.5	66.96	33.04	586.24
		3	67.1	32.9	597.14
	10	1.5	66.27	33.73	600.45
		3	67.97	32.03	609.64
	30	1.5	66.87	33.13	620.54
		3	67.38	32.62	632.18
$Fe_2(SO_4)_3$	5	1.5	71.17	28.83	583.54
		3	68.86	31.14	596.72
	10	1.5	67.3	32.7	595.53
		3	66.77	33.23	605.62
	30	1.5	67.22	32.78	620.81
		3	66.95	33.05	634.39

including the expected activation energy (Ea), the pre-exponential factor (A), the proportionality constant (c), the standard deviation (σ) characterizing the distribution of activation energies, and the standard error of the fit (SE).

Fig. 2a-c shows the activation energies for the pyrolysis of the three pseudo-components at three heating rates. The computed activation energy values range from 154 kJ/mol to 181 kJ/mol for the first pseudo-component, 167 kJ/mol to 203 kJ/mol for the second pseudo-component, and 25.6 kJ/mol to 51.0 kJ/mol for the third pseudo-component. These findings align with data garnered from previous investigations on diverse biomass types employing the DAEM model. Moreover, the characteristic range for the corresponding pre-exponential factor spans from 10^4 to 10^{14} s^{-1}, while the characteristic range for activation energy extends from 50 to 350 kJ/mol [36,57].

On the contrary, the outcomes of the DAEM model reveal that the heating rate exerts negligible influence on the activation energy governing the pyrolysis of cocoa shell's three macro-components. In contrast, the introduction of iron sulfate markedly impacts the activation energies associated with the three macro-components: a consistent elevation in activation energy is observed across all three heating rates. In the case of zinc sulfate, a marginal reduction in the activation energy during the decomposition of the third pseudo-component is observed, though it lacks statistical significance. Furthermore, no substantial alterations in activation energies for the decomposition of the first and second pseudo-components are evident in the presence of this catalyst.

Statistical analyses validate the findings above. The catalyzed pyrolysis of cocoa shells with ferric sulfate distinctly demonstrates the catalyst's significant influence on the activation energies governing reactions of the three pseudo-components, as well as on the standard deviations characterizing the distribution of activation energies. This is evident across all components, except for the standard deviation for the second pseudo-component (E_{01}, $P = 0.0036$; S_1, $P = 0.0070$; E_{02}, $P = 0.0083$; E_{03}, $P = 0.0118$; and S_3, $P = 0.0065$). In contrast, the activation energies associated with the decomposition of cocoa shell pseudo-components remain unaltered in

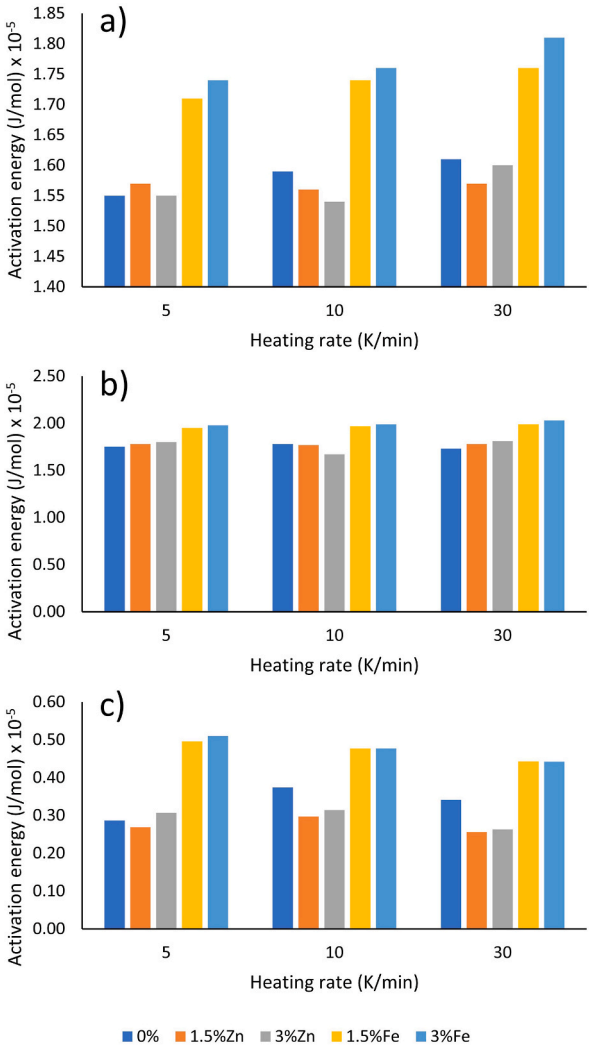

Fig. 2. Activation energies obtained from the fitting of the DAEM model with three sets of reactions to the DTG data of cocoa shell pyrolysis at a heating rate of **a)** 5 K/min, **b)** 10 K/min, and **c)** 30 K/min.

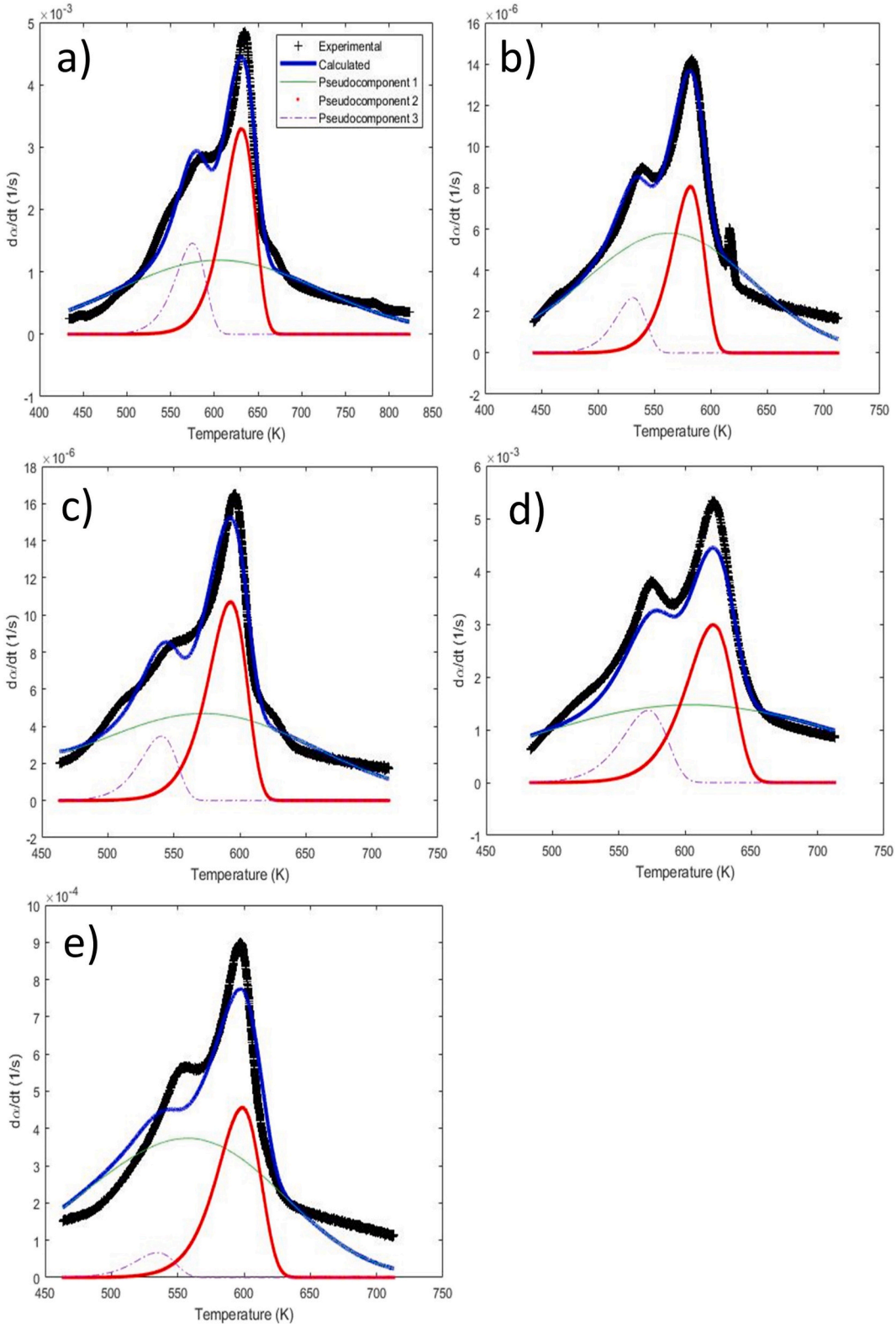

Fig. 3. Fitting of the DAEM model with three sets of reactions to the DTG data of cocoa shell pyrolysis at a heating rate of 5 K/min **a).** Cocoa Shell without catalysts **b).** Cocoa Shell +1.5 % $Fe_2(SO_4)_3$ **c).** Cocoa shell +3 % $Fe_2(SO_4)_3$ **d).** Cocoa Shell +1.5 % $ZnSO_4$ **e).** Cocoa shell +3 % $ZnSO_4$.

the presence of zinc sulfate, displaying no statistically significant changes.

Studies employing higher concentrations of Zn (5 %) demonstrated that this element inhibits hemicellulose fragmentation reactions and promotes the thermal decomposition of cellulose, which was attributed to heat transfer effects [19]. On the other hand, other results align with the findings obtained in this study, where the zinc cation exhibited no catalytic or inhibitory effects on biomass pyrolysis [21]. The discrepancy in results suggests a strong dependence of the effects of the studied sulfates on the raw material, as also suggested by Alvarez in the investigation of the effect of ferric sulfate on the properties of biochar obtained from catalytic pyrolysis of biomass residues [26].

Fig. 3(a–e), 4(a-e), and 5(a-e) show the fit of the DAEM model with three pseudo-components to the experimental DTG curves for different catalyst percentages and heating rates in the pyrolysis of cocoa shells. In this study, we attributed the first pseudo-component to the thermal breakdown of lignin and residual carbohydrate fractions, characterized by a broadened temperature range of decomposition. The second pseudo-component was ascribed to the devolatilization of cellulose, while the third pseudo-component encapsulated hemicellulose pyrolysis, distinguished by its propensity to engage in reactions at lower temperatures [56]. These

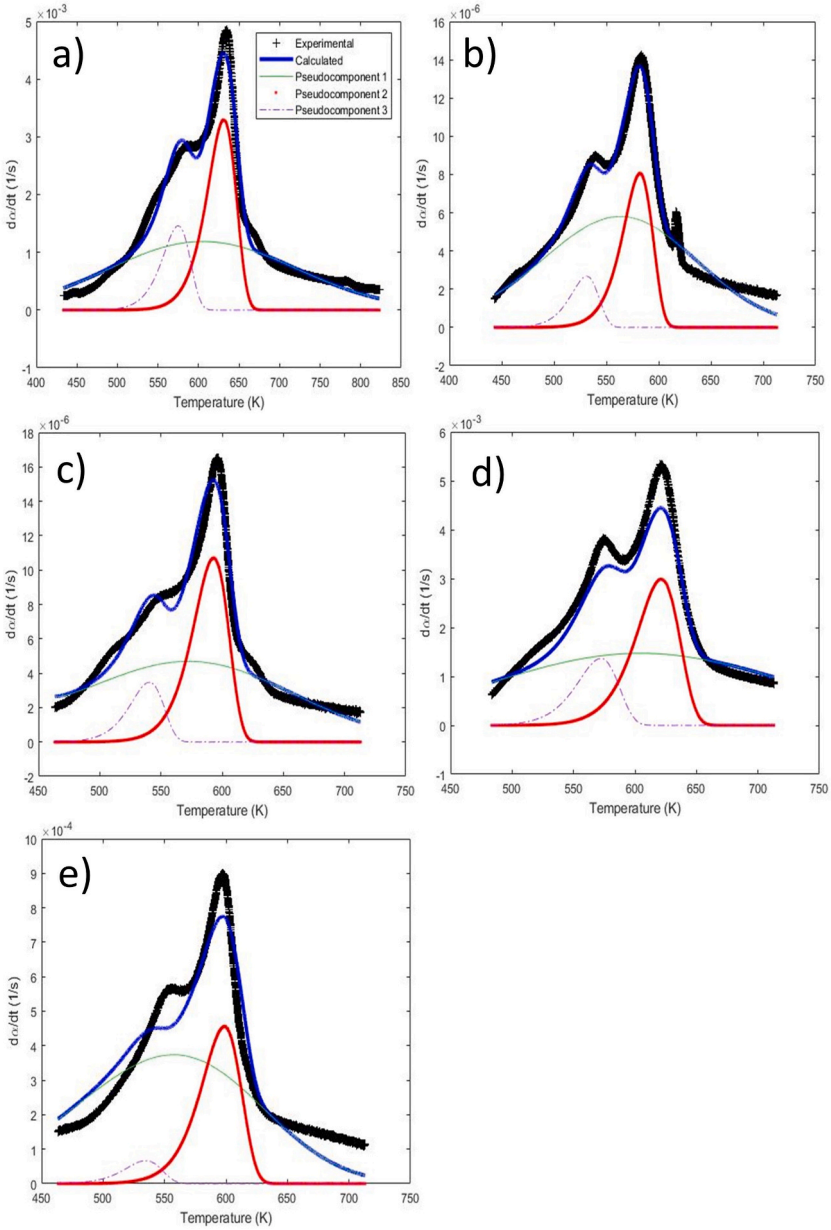

Fig. 4. Fitting of the DAEM model with three sets of reactions to the DTG data of cocoa shell pyrolysis at a heating rate of 10 K/min **a).** Cocoa Shell without catalysts **b).** Cocoa Shell +1.5 % $Fe_2(SO_4)_3$ **c).** Cocoa shell +3 % $Fe_2(SO_4)_3$ **d).** Cocoa Shell +1.5 % $ZnSO_4$ **e).** Cocoa shell +3 % $ZnSO_4$.

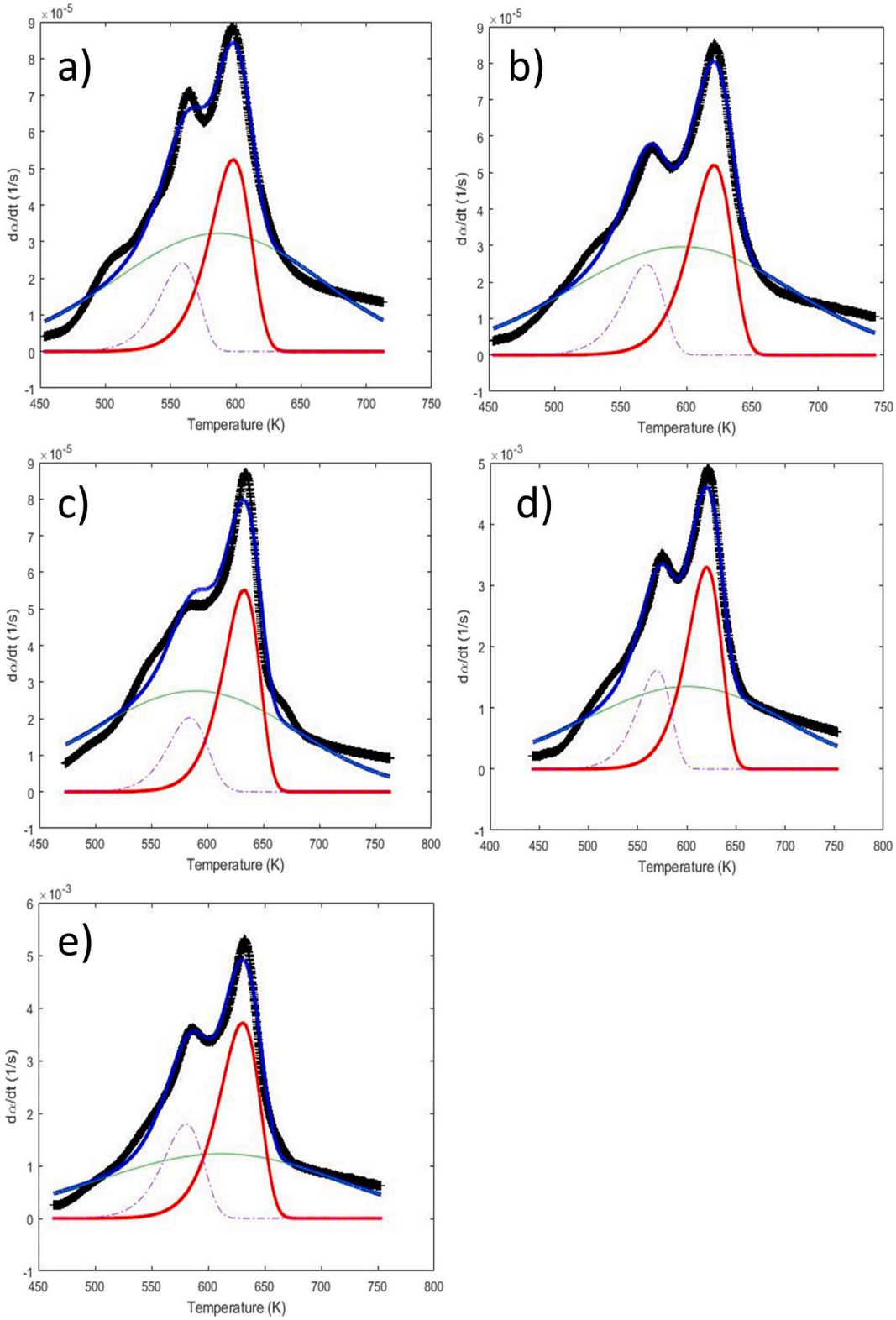

Fig. 5. Fitting of the DAEM model with three sets of reactions to the DTG data of cocoa shell pyrolysis at a heating rate of 30 K/min **a).** Cocoa Shell without catalysts **b).** Cocoa Shell +1.5 % $Fe_2(SO_4)_3$ **c).** Cocoa shell +3 % $Fe_2(SO_4)_3$ **d).** Cocoa Shell +1.5 % $ZnSO_4$ **e).** Cocoa shell +3 % $ZnSO_4$.

curves are designated as follows: the first pseudo-component, representative of lignin, is delineated in green; the second pseudo-component, embodying cellulose, is depicted in red; lastly, the third pseudo-component, indicative of hemicellulose, is represented by the purple curve.

3.4. Analysis of the evolved gases

Through simultaneous Thermogravimetric Analysis-Fourier Transform Infrared Spectroscopy (TGA-FTIR), real-time monitoring of the gaseous products generated during the pyrolysis of cocoa shell residues was achieved. These findings are illustrated in three-dimensional plots (Fig. 6 and supplementary material), delineating changes in the infrared spectra of the evolved gases relative to pyrolysis temperature. For an in-depth scrutiny of the gas characteristics, Fig. 7a-d portrays the infrared spectra of gaseous products resulting from cocoa shell pyrolysis at two pivotal temperatures, as identified in Fig. 3, where a bimodal peak pattern is evident. The higher peak, distinctly attributed to the thermal decomposition of cellulose, holds significance as it represents the temperature with the most rapid conversion of cellulose into products. This feature aids in its discernment. Likewise, the lower peak, henceforth referred to as the shoulder temperature, garners equal importance for analogous reasons elucidated earlier, albeit related to the degradation of hemicellulose into products.

Figs. 7–9 present the selected FTIR spectra of the evolved gases acquired in proximity to the temperatures corresponding to the peaks of maximal mass loss. These spectra were normalized relative to the carbon dioxide peak height (Table S2). Fig. 7 offers a glimpse into the FTIR spectra acquired at a heating rate of 5 K/min.

In Fig. 7a, the discernible influence of ferric sulfate is evident in the reduction of H_2O/CO_2 and CH_4/CO_2 ratios at temperatures corresponding to the peak of the highest mass loss rate. The presence of 1.5 % ferric sulfate introduces heightened stresses associated with nitrogen compounds (-CN) during both events, characterized by the highest and second-highest mass loss rates (Fig. 7b). However, in the event with the second-highest mass loss rate, a notable augmentation in the H_2O/CO_2 ratio is observed when cocoa shell pyrolysis occurs in the presence of 3 % ferric sulfate. This stands in stark contrast to the pyrolysis within the temperature range of the highest mass loss, signifying a distinctive impact of ferric sulfate on the pyrolysis of cellulose and hemicellulose at this heating rate.

Conversely, Fig. 7c elucidates the impact of zinc sulfate on the FTIR spectra of the evolved gases, precisely at temperatures corresponding to the event with the highest mass loss rate and a heating rate of 10 K/min. A parallel trend to that observed for ferric sulfate emerges, characterized by a reduction in the H_2O/CO_2 and CH_4/CO_2 ratios, and an elevation in nitrogen compounds concentration. In Fig. 7d, corresponding to the FTIR spectra of gases evolved at temperatures indicative of the thermal event with the second-highest mass loss rate, a marked shift is observed in the proportions of bands correlated with the ratios of intensities in stretching vibrations, namely CO/CO_2, H_2O/CO_2, –COO–/CO_2, and –CN/CO_2, specifically evident at a 3 % zinc sulfate concentration. Once more, this highlights a distinct catalytic effect, in this instance, exerted by zinc sulfate, on the thermal decomposition of cellulose and hemicellulose.

Fig. 8(a–d) depicts spectra equivalent to those in Fig. 7, but at a heating rate of 10 K/min. In the presence of ferric sulfate, a discernible rise in H_2O/CO_2, –COO–/CO_2, and –CN/CO_2 ratios is noted with escalating catalyst concentration for the two studied thermal events (Fig. 8a and b). Concurrently, a decrement in the intensity ratio of CH_4/CO_2 bands is observed, with a more pronounced effect during hemicellulose pyrolysis. With zinc sulfate, emphasis is placed on the reduction of the CH_4/CO_2 ratio and heightened presence of oxygenated compounds in both events (Fig. 8c and d), along with an augmented intensity ratio of –CN/CO_2 bands within the temperature range indicative of hemicellulose thermal decomposition.

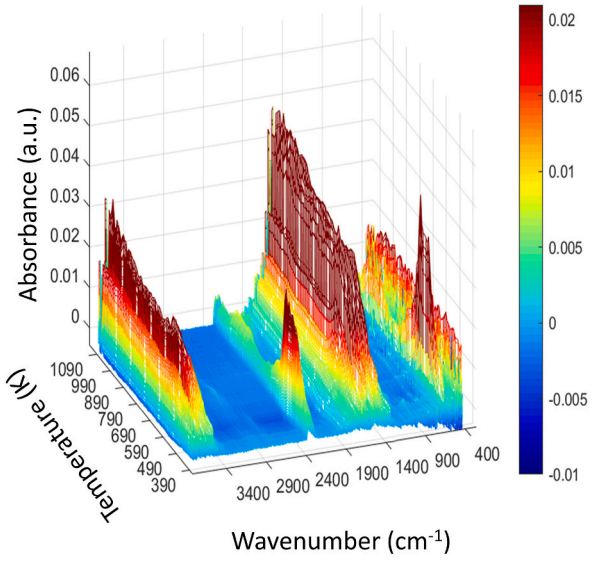

Fig. 6. 3D IR spectra of gases evolved during the pyrolysis of cocoa shell +3 % $Zn(SO)_4$ heated at 5 K/min.

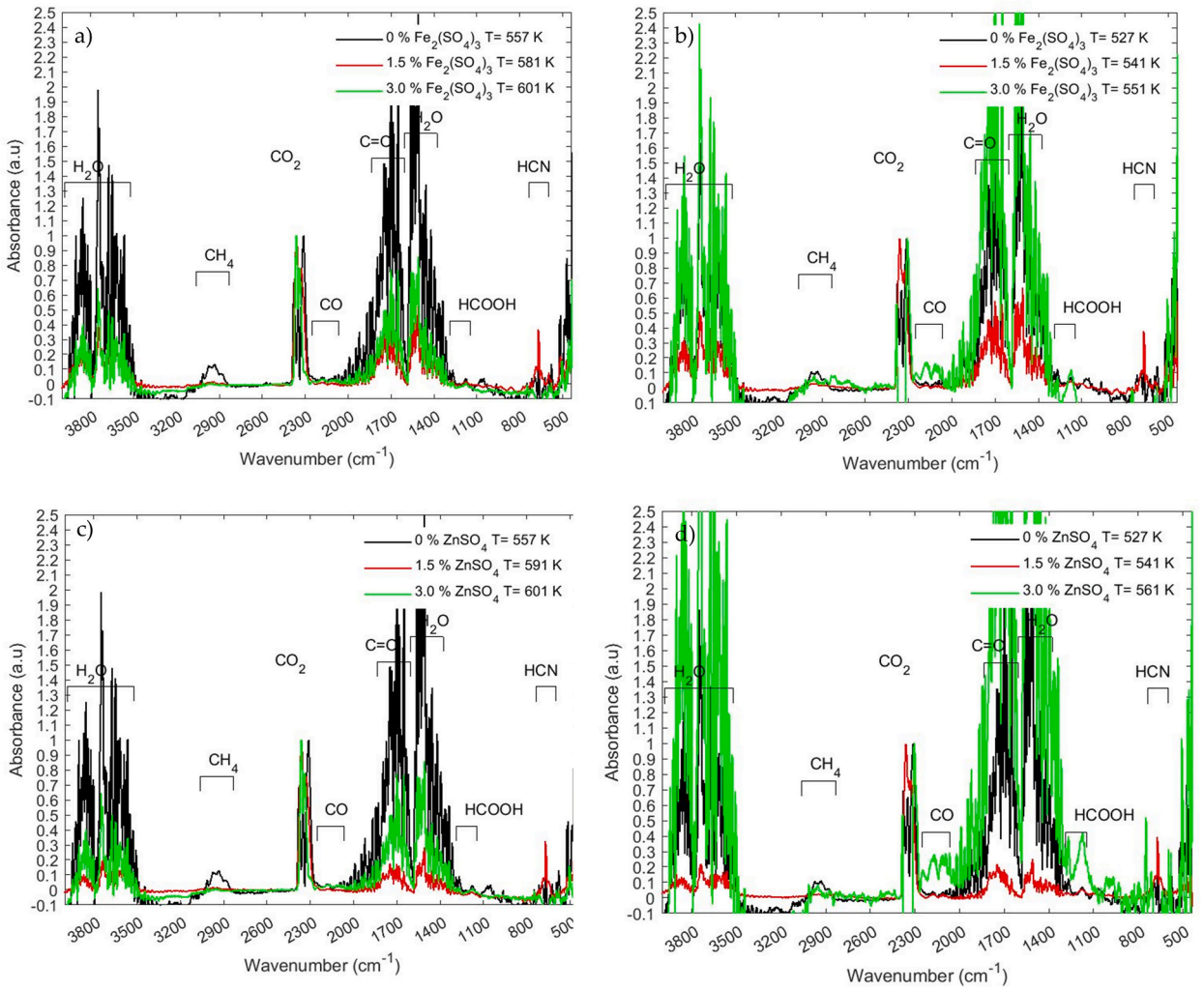

Fig. 7. IR spectra of gases evolved during pyrolysis at heating rates of 5 K/min **a)** Cocoa shells + $Fe_2(SO_4)_3$ at temperatures of the maxima of mass loss, **b)** Cocoa shells + $Fe_2(SO_4)_3$ at temperatures of the second maxima of mass loss **c)** Cocoa shells + $Zn(SO)_4$ at temperatures of the maxima of mass loss, **b)** Cocoa shells + $Zn(SO)_4$ at temperatures of the second maxima of mass loss.

Fig. 9a-d mirrors the spectra in Fig. 7(a–d) and 8(a-d), hitherto with a heating rate of 30 K/min. At this heating rate, the concentration of evolved species surpasses that of spectra obtained at 5 K/min and 10 K/min, resulting in sharper and more defined spectra. In Fig. 9a, a decrease in the intensity ratios of CH_4/CO_2, H_2O/CO_2, and CO/CO_2 stretching modes is confirmed, as well as an escalation in the intensities of C═O/CO_2, COO/CO_2, and –CN/CO_2 in the presence of ferric sulfate during cellulose decomposition. Conversely, for hemicellulose decomposition, an upswing in the CO/CO_2 and C═O/CO_2 ratios is observed (Fig. 9b). Meanwhile, zinc sulfate leads to an augmentation in the intensity ratios of H_2O/CO_2, C═O/CO_2, and HCN/CO_2 coupled with a reduction in the intensity ratios of CH_4/CO_2 and CO/CO_2 at temperatures around cellulose thermal decomposition (Fig. 9c). In hemicellulose thermal decomposition (Fig. 9d), zinc sulfate amplifies the intensity ratios of C═O/CO_2, H_2O/CO_2, and COO/CO_2 stretching modes.

In the infrared spectra presented in Figs. 7–9, prominent gaseous products arising from cocoa shell pyrolysis include CO_2, CH_4, CO, and H_2O, along with organic compounds such as acids (R–COOH). Notably, water absorption bands manifest within the ranges of 3750-3500 cm^{-1} and 1700-1400 cm^{-1}. CO_2 is discernible within bands spanning 2400-2200 cm^{-1}, attributed to the decomposition and reforming of carboxyl functional groups (C═O). CO is observed within the 2200-2000 cm^{-1} range, resulting from the breakdown of carbonyl groups (C–*O*–C) and other compounds featuring CH bonds, induced by the cleavage of methoxyl and methylene groups (CH3) [58]. Distinctive bands in the 1900-1700 cm^{-1} and 1200-1100 cm^{-1} ranges correspond to R–COOH compounds. Finally, the presence of HCN is identified between bands at 790-650 cm^{-1}.

Fig. 7(a–d), 8(a-d), and 9(a-d) show the infrared profiles of the evolved gases at temperatures corresponding to the peaks under varying percentages of the catalysts studied. These profiles provide insights into the occurrence of decarboxylation reactions within the biomass macro-components at elevated temperatures. Furthermore, secondary gas-phase reactions are induced by the rupture of weak aliphatic bonds, resulting in the production of carbon dioxide [59,60]. Notably, the impact of these catalysts on cellulose is

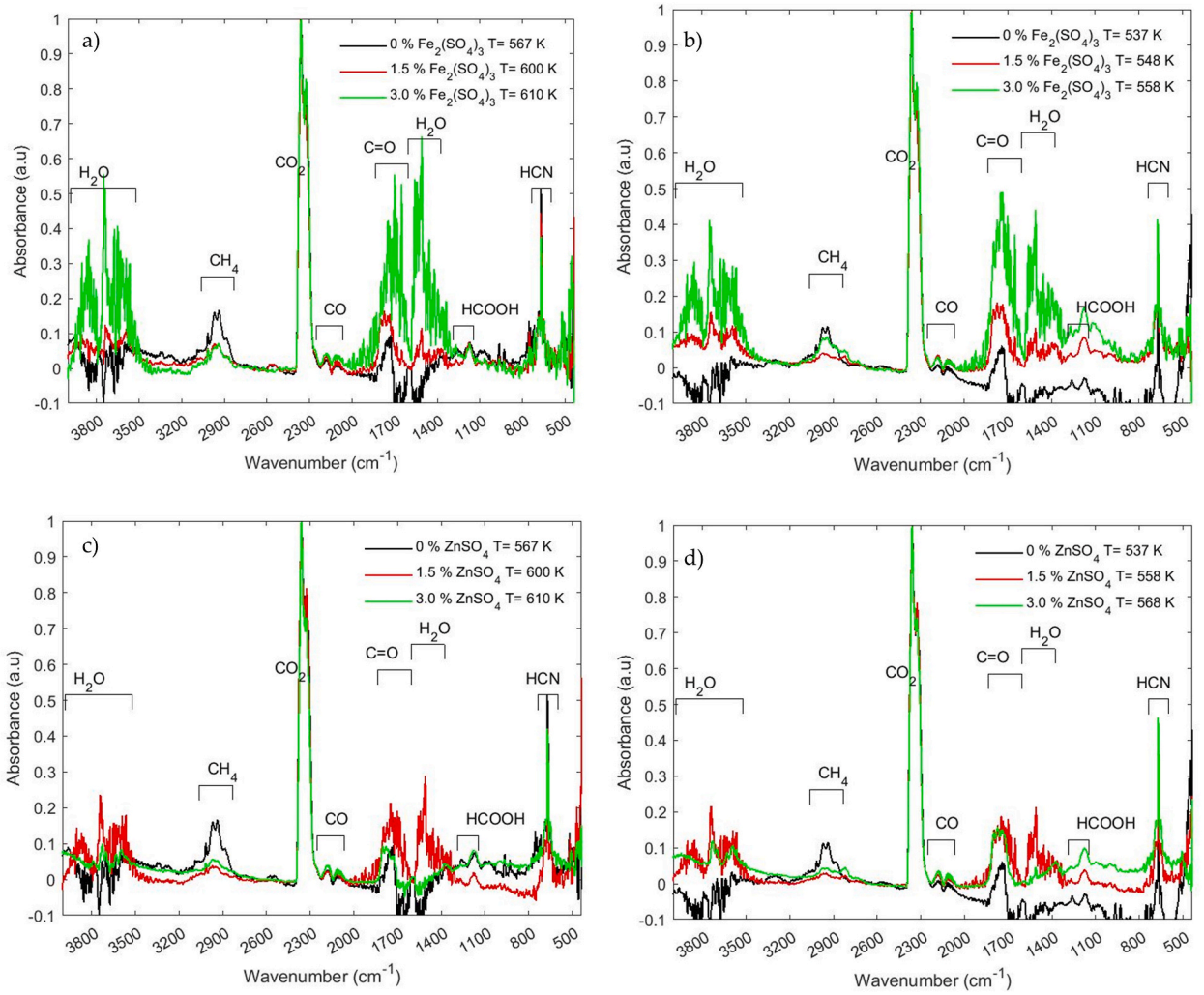

Fig. 8. IR spectra of gases evolved during pyrolysis at heating rates of 10 K/min **a)** Cocoa shells + $Fe_2(SO_4)_3$ at temperatures of the maxima of mass loss, **b)** Cocoa shells + $Fe_2(SO_4)_3$ at temperatures of the second maxima of mass loss **c)** Cocoa shells + $Zn(SO)_4$ at temperatures of the maxima of mass loss, **b)** Cocoa shells + $Zn(SO)_4$ at temperatures of the second maxima of mass loss.

underscored by an increase in carbonization, elevated peak temperatures, and the second pseudo-component decomposition (Table S2).

Both catalysts induced alterations in the infrared spectra of the evolved gases, primarily evident in the relative intensities of bands corresponding to the stretching vibrations of constituent groups within CO_2, CO, water, and oxygenated compounds. This implies that both catalysts modulate the concentrations of compounds released in the evolved gases, albeit without generating novel compounds. Similar shifts in product distribution have been noted in the pyrolysis of other biomasses under the influence of these catalysts, despite their protective or negligible impact on kinetic parameters [22,24,25,52]. Protective effects of these metals on cellulose have been suggested by Refs. [21,26]. On the other hand [19], proposes that metals like zinc favor multimolecular repolymerization reactions and an increased production of oxygenated compounds such as furfural. This is reflected in the reduction of non-oxygenated compounds, as shown in the infrared spectra of the evolved gases, and in the emergence of more prominent peaks related to oxygenated compounds when either ferric or zinc sulfate are impregnated in the biomass, as observed in Figs. 7–9.

4. Conclusions

The pyrolysis of cocoa shell residues was studied in the presence and absence of iron and zinc sulfates using EGA. The results were fitted to the DAEM model, allowing for the interpretation of the catalytic effect on the decomposition of hemicellulose, cellulose, and lignin, the major components of the biomass under study. The DTG profiles demonstrate an increase in pyrolysis temperatures in the presence of ferric sulfate. It was observed that within the studied composition range, ferric sulfate exerts an inhibitory effect on the decomposition of all three macro-components of cocoa shell. On the other hand, zinc sulfate did not exhibit any significant effect on the

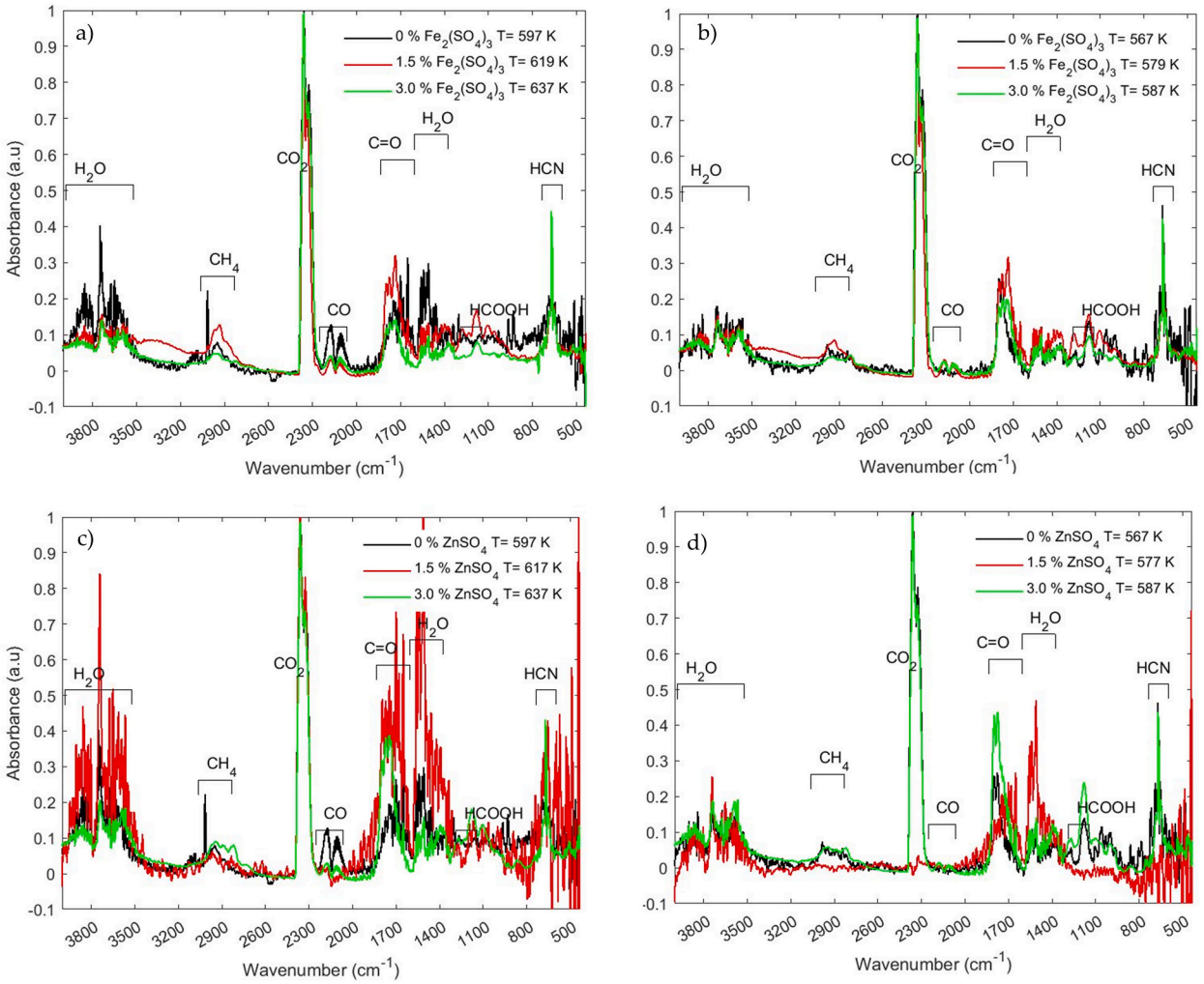

Fig. 9. IR spectra of gases evolved during pyrolysis at heating rates of 30 K/min **a)** Cocoa shells + $Fe_2(SO_4)_3$ at temperatures of the maxima of mass loss, **b)** Cocoa shells + $Fe_2(SO_4)_3$ at temperatures of the second maxima of mass loss **c)** Cocoa shells + $Zn(SO)_4$ at temperatures of the maxima of mass loss, **b)** Cocoa shells + $Zn(SO)_4$ at temperatures of the second maxima of mass loss.

biomass decomposition kinetics: ferric sulfate had a significant influence on the activation energies governing reactions of the three pseudo-components, as well as on the standard deviations characterizing the distribution of activation energies. In contrast, the activation energies associated with the decomposition of cocoa shell pseudo-components remain unaltered in the presence of zinc sulfate, displaying no statistically significant changes.

TG-FTIR analysis indicated that the main gases released from thermal decomposition were CO_2, H_2O, CH_4, CO, and HCN compounds, and oxygenated compounds such as HCOOH and CH_3COOH. Both catalysts induced alterations in the infrared spectra of the evolved gases, primarily manifested in the relative intensities of bands corresponding to the stretching vibrations of constituent groups within CO_2, CO, water, and oxygenated compounds. Additionally, the FTIR spectra of the evolved gases reveal a reduction in the concentration of hydrocarbon-type compounds such as methane and an elevation in the concentration of oxygenated compounds when either $ZnSO_4$ or $Fe_2(SO_4)_3$ was present. These salts could be applied in biorefineries where the primary products are oxygenated compounds like acids, aldehydes, or ketones.

CRediT authorship contribution statement

Angie Xiomara Vesga: Writing – original draft, Validation, Investigation. **María Fernanda Cuentas:** Writing – original draft, Validation, Investigation. **Alberto Ricardo Albis Arrieta:** Writing – review & editing, Supervision, Resources, Methodology, Formal analysis, Conceptualization.

Declaration of generative AI and AI-assisted technologies in the writing process

During the preparation of this work the author(s) used ChatGPT in order to check grammar and improve writing. After using this tool/service, the author(s) reviewed and edited the content as needed and take(s) full responsibility for the content of the publication.

Declaration of competing interest

The authors declare that they have no known competing financial interests or personal relationships that could have appeared to influence the work reported in this paper.

Appendix A. Supplementary data

Supplementary data to this article can be found online at https://doi.org/10.1016/j.heliyon.2024.e33117.

References

[1] Z. Liu, H.B. Saydaliev, J. Lan, S. Ali, M.K. Anser, Assessing the effectiveness of biomass energy in mitigating CO2 emissions: Evidence from Top-10 biomass energy consumer countries, Renew. Energy 191 (May 2022) 842–851, https://doi.org/10.1016/J.RENENE.2022.03.053.

[2] D. Gamaralalage, et al., Life cycle assessment of international biomass utilization: a case study of Malaysian palm kernel shells for biomass power generation in Japan, Waste Biomass Valorization 13 (5) (May 2022) 2717–2733, https://doi.org/10.1007/s12649-021-01643-3.

[3] E.O.K. Oddoye, C.K. Agyente-Badu, E. Gyedu-Akoto, Cocoa and its by-products: identification and utilization, in: R. Watson, V. Preedy, S. Zibadi (Eds.), Chocolate in Health and Nutrition, vol. 7, Humana Press, Totowa, 2013, pp. 23–37.

[4] M. Ganesapillai, et al., Waste to energy: a review of biochar production with emphasis on mathematical modelling and its applications, Heliyon 9 (4) (Apr. 2023) e14873, https://doi.org/10.1016/j.heliyon.2023.e14873.

[5] L. Zhang, R. Liu, R. Yin, Y. Mei, Upgrading of bio-oil from biomass fast pyrolysis in China: a review, Renew. Sustain. Energy Rev. 24 (Aug. 2013) 66–72, https://doi.org/10.1016/J.RSER.2013.03.027.

[6] Z. Han, Z. Guo, Y. Zhang, X. Xiao, Z. Xu, Y. Sun, Pyrolysis characteristics of biomass impregnated with cadmium, copper and lead: influence and distribution, Waste Biomass Valorization 9 (7) (Jul. 2018) 1223–1230, https://doi.org/10.1007/s12649-017-0036-5.

[7] A. Khelfa, A. Bensakhria, J.V. Weber, Investigations into the pyrolytic behaviour of birch wood and its main components: primary degradation mechanisms, additivity and metallic salt effects, J. Anal. Appl. Pyrolysis 101 (May 2013) 111–121, https://doi.org/10.1016/j.jaap.2013.02.004.

[8] D. Lv, M. Xu, X. Liu, Z. Zhan, Z. Li, H. Yao, Effect of cellulose, lignin, alkali and alkaline earth metallic species on biomass pyrolysis and gasification, Fuel Process. Technol. 91 (8) (Aug. 2010) 903–909, https://doi.org/10.1016/j.fuproc.2009.09.014.

[9] A. Kumar, S.V.P. Mylapilli, S.N. Reddy, Thermogravimetric and kinetic studies of metal (Ru/Fe) impregnated banana pseudo-stem (Musa acuminate), Bioresour. Technol. 285 (Aug. 2019) 121318, https://doi.org/10.1016/j.biortech.2019.121318.

[10] Z. Cao, J. Niu, Y. Gu, R. Zhang, Y. Liu, L. Luo, Catalytic pyrolysis of rice straw: screening of various metal salts, metal basic oxide, acidic metal oxide and zeolite catalyst on products yield and characterization, J. Clean. Prod. 269 (Oct. 2020) 122079, https://doi.org/10.1016/j.jclepro.2020.122079.

[11] S. Zhao, M. Liu, L. Zhao, J. Lu, Effects of organic and inorganic metal salts on thermogravimetric pyrolysis of biomass components, Kor. J. Chem. Eng. 34 (12) (Dec. 2017) 3077–3084, https://doi.org/10.1007/s11814-017-0209-8.

[12] G. Dobele, G. Rossinskaja, T. Dizhbite, G. Telysheva, D. Meier, O. Faix, Application of catalysts for obtaining 1,6-anhydrosaccharides from cellulose and wood by fast pyrolysis, J. Anal. Appl. Pyrolysis 74 (1–2) (Aug. 2005) 401–405, https://doi.org/10.1016/j.jaap.2004.11.031.

[13] B. Li, et al., Catalysis/CO2 sorption enhanced pyrolysis-gasification of biomass for H2-rich gas production: effects of activated carbon, NiO active component and calcined dolomite, Fuel 334 (Feb. 2023) 126842, https://doi.org/10.1016/j.fuel.2022.126842.

[14] S.A. Rollag, J.K. Lindstrom, R.C. Brown, Pretreatments for the continuous production of pyrolytic sugar from lignocellulosic biomass, Chem. Eng. J. 385 (Apr. 2020) 123889, https://doi.org/10.1016/j.cej.2019.123889.

[15] B. Li, C.F. Magoua Mbeugang, Y. Huang, D. Liu, Q. Wang, S. Zhang, A review of CaO based catalysts for tar removal during biomass gasification, Energy 244 (Apr. 2022) 123172, https://doi.org/10.1016/j.energy.2022.123172.

[16] W.-H. Chen, et al., Catalytic level identification of ZSM-5 on biomass pyrolysis and aromatic hydrocarbon formation, Chemosphere 271 (May 2021) 129510, https://doi.org/10.1016/j.chemosphere.2020.129510.

[17] C.-H. Zhou, X. Xia, C.-X. Lin, D.-S. Tong, J. Beltramini, Catalytic conversion of lignocellulosic biomass to fine chemicals and fuels, Chem. Soc. Rev. 40 (11) (2011) 5588, https://doi.org/10.1039/c1cs15124j.

[18] D.Y. Rachel-Tang, A. Islam, Y.H. Taufiq-Yap, Bio-oil production via catalytic solvolysis of biomass, RSC Adv. 7 (13) (2017) 7820–7830, https://doi.org/10.1039/C6RA27824H.

[19] C. Li, et al., Influencing mechanism of zinc mineral contamination on pyrolysis kinetic and product characteristics of corn biomass, J Environ Manage 281 (Mar. 2021) 111837, https://doi.org/10.1016/j.jenvman.2020.111837.

[20] Q. Zhou, S. Yang, H. Wang, Z. Liu, L. Zhang, Selective deoxygenation of biomass volatiles into light oxygenates catalysed by S-doped, nanosized zinc-rich scrap tyre char with in-situ formed multiple acidic sites, Appl. Catal., B 282 (Mar. 2021) 119603, https://doi.org/10.1016/j.apcatb.2020.119603.

[21] Z.A. Mayer, A. Apfelbacher, A. Hornung, Effect of sample preparation on the thermal degradation of metal-added biomass, J. Anal. Appl. Pyrolysis 94 (Mar. 2012) 170–176, https://doi.org/10.1016/j.jaap.2011.12.008.

[22] M.A. Suárez Useche, Y. Castillo Santiago, J.B. Restrepo, A.R. Albis Arrieta, K.P. Agámez Salgado, Evaluation of the zinc sulfate catalytic effect in empty fruit bunches pyrolysis, Processes 10 (9) (Sep. 2022) 1748, https://doi.org/10.3390/pr10091748.

[23] G.N. Richards, G. Zheng, Influence of metal ions and of salts on products from pyrolysis of wood: applications to thermochemical processing of newsprint and biomass, J. Anal. Appl. Pyrolysis 21 (1–2) (Sep. 1991) 133–146, https://doi.org/10.1016/0165-2370(91)80021-Y.

[24] A. Albis, É. Ortiz, I. Piñeres, J. Osorio, J. Monsalvo, Pirólisis de hemicelulosa catalizada por sulfato de zinc y sulfato férrico, Revista ION 31 (2) (Jan. 2019) 37–49, https://doi.org/10.18273/revion.v31n2-2018003.

[25] A.R. Albis Arrieta, E. Ortiz Muñoz, I.E. Piñeres Ariza, J.S. Osorio Cardozo, J. Monsalvo Morales, Efecto catalítico del sulfato de zinc y el sulfato férrico en la pirólisis de la lignina/Catalytic effect of zinc sulfate and ferric sulfate on lignin pyrolysis, Prospectiva 16 (1) (Dec. 2017) 41–50, https://doi.org/10.15665/rp.v16i1.1397.

[26] M.L. Álvarez, G. Gascó, T. Palacios, J. Paz-Ferreiro, A. Méndez, Fe oxides-biochar composites produced by hydrothermal carbonization and pyrolysis of biomass waste, J. Anal. Appl. Pyrolysis 151 (Oct. 2020) 104893, https://doi.org/10.1016/j.jaap.2020.104893.

[27] L.A. Edye, G.N. Richards, G. Zheng, Transition Metals as Catalysts for Pyrolysis and Gasification of Biomass, 1992, pp. 90–101, https://doi.org/10.1021/bk-1992-0515.ch008.

[28] T. Dickerson, J. Soria, Catalytic fast pyrolysis: a review, Energies 6 (1) (Jan. 2013) 514–538, https://doi.org/10.3390/en6010514.

[29] A. Martinez, L. Meriño, A. Albis, J. Ortega, Comparative study of the reaction kinetics of three residual biomasses, Bioresources 16 (2) (Mar. 2021) 2891–2905, https://doi.org/10.15376/biores.16.2.2891-2905.

[30] G. Várhegyi, Z. Czégény, E. Jakab, K. McAdam, C. Liu, Tobacco pyrolysis. Kinetic evaluation of thermogravimetric–mass spectrometric experiments, J. Anal. Appl. Pyrolysis 86 (2) (Nov. 2009) 310–322, https://doi.org/10.1016/J.JAAP.2009.08.008.

[31] Y. K N, et al., Lignocellulosic biomass-based pyrolysis: a comprehensive review, Chemosphere 286 (Jan. 2022) 131824, https://doi.org/10.1016/J.CHEMOSPHERE.2021.131824.

[32] T. Kan, V. Strezov, T.J. Evans, Lignocellulosic biomass pyrolysis: a review of product properties and effects of pyrolysis parameters, Renew. Sustain. Energy Rev. 57 (May 2016) 1126–1140, https://doi.org/10.1016/J.RSER.2015.12.185.

[33] A.A. Lappas, K.G. Kalogiannis, E.F. Iliopoulou, K.S. Triantafyllidis, S.D. Stefanidis, Catalytic pyrolysis of biomass for transportation fuels, Wiley Interdiscip Rev Energy Environ 1 (3) (Nov. 2012) 285–297, https://doi.org/10.1002/wene.16.

[34] P. De Filippis, B. de Caprariis, M. Scarsella, N. Verdone, Double distribution activation energy model as suitable tool in explaining biomass and coal pyrolysis behavior, Energies 8 (3) (Mar. 2015) 1730–1744, https://doi.org/10.3390/en8031730.

[35] G.-M. Kim, D.-G. Lee, C.-H. Jeon, Fundamental characteristics and kinetic analysis of lignocellulosic woody and herbaceous biomass fuels, Energies 12 (6) (Mar. 2019) 1008, https://doi.org/10.3390/en12061008.

[36] J. Cai, W. Wu, R. Liu, An overview of distributed activation energy model and its application in the pyrolysis of lignocellulosic biomass, Renew. Sustain. Energy Rev. 36 (Aug. 2014) 236–246, https://doi.org/10.1016/j.rser.2014.04.052.

[37] H. Liu, M.S. Ahmad, H. Alhumade, A. Elkamel, S. Sammak, B. Shen, A hybrid kinetic and optimization approach for biomass pyrolysis: the hybrid scheme of the isoconversional methods, DAEM, and a parallel-reaction mechanism, Energy Convers. Manag. 208 (Mar. 2020) 112531, https://doi.org/10.1016/j.enconman.2020.112531.

[38] M. Radojević, B. Janković, V. Jovanović, D. Stojiljković, N. Manić, Comparative pyrolysis kinetics of various biomasses based on model-free and DAEM approaches improved with numerical optimization procedure, PLoS One 13 (10) (Oct. 2018) e0206657, https://doi.org/10.1371/journal.pone.0206657.

[39] M. Güneş, S. Güneş, A direct search method for determination of DAEM kinetic parameters from nonisothermal TGA data (note), Appl. Math. Comput. 130 (2–3) (Aug. 2002) 619–628, https://doi.org/10.1016/S0096-3003(01)00124-2.

[40] V.T. Ciuryla, R.F. Weimer, D.A. Bivans, S.A. Motika, Ambient-pressure thermogravimetric characterization of four different coals and their chars, Fuel 58 (10) (Oct. 1979) 748–754, https://doi.org/10.1016/0016-2361(79)90075-9.

[41] D.S. Thakur, H.E. Nuttall, Kinetics of pyrolysis of Moroccan oil shale by thermogravimetry, Ind. Eng. Chem. Res. 26 (7) (Jul. 1987) 1351–1356, https://doi.org/10.1021/ie00067a015.

[42] S. Tia, S.C. Bhattacharya, P. Wibulswas, Thermogravimetric analysis of Thai lignite—I. pyrolysis kinetics, Energy Convers. Manag. 31 (3) (Jan. 1991) 265–276, https://doi.org/10.1016/0196-8904(91)90080-3.

[43] A.G. Nerheim, Applications of spectral techniques to thermal analysis, in: J.R. Ferraro, L.J. Basile (Eds.), Transform Infrared Spectroscopy: Applications to Chemical Systems, vol. 4, Academic Press, Orlando, 2012, pp. 147–167.

[44] A. Albis, E. Ortiz, A. Suárez, I. Piñeres, TG/MS study of the thermal devolatization of Copoazú peels (Theobroma grandiflorum), J. Therm. Anal. Calorim. 115 (1) (Jan. 2014) 275–283, https://doi.org/10.1007/s10973-013-3227-8.

[45] A. Bhargava, P. van Hees, B. Andersson, Pyrolysis modeling of PVC and PMMA using a distributed reactivity model, Polym Degrad Stab 129 (Jul. 2016) 199–211, https://doi.org/10.1016/j.polymdegradstab.2016.04.016.

[46] A.R. Albis Arrieta, M. Colón Castro, M. Quintero Parra, Efecto catalítico del Na2CO3 sobre la pirólisis de los residuos del sorgo (Sorghum bicolor L. Moench), Prospectiva 19 (1) (2021) 1–18.

[47] D. Lock Navarro, Potencial energético de los residuos de la cadena de valor del cacao (Theobroma cacao) en la Región Madre De Dios, Undergraduate, Universidad Nacional Agraria La Molina, Lima (2018), 86 pages.

[48] A. van der Drift, J. van Doorn, J.W. Vermeulen, Ten residual biomass fuels for circulating fluidized-bed gasification, Biomass Bioenergy 20 (1) (Jan. 2001) 45–56, https://doi.org/10.1016/S0961-9534(00)00045-3.

[49] J.O. Titiloye, M.S. Abu Bakar, T.E. Odetoye, Thermochemical characterisation of agricultural wastes from West Africa, Ind. Crops Prod. 47 (May 2013) 199–203, https://doi.org/10.1016/j.indcrop.2013.03.011.

[50] O. Kitani, C.W. Hall, Biomass Handbook, Gordon and Breach Science Publishers, New York, 1989, https://doi.org/10.1080/00908319108956421.

[51] K. Açıkalın, Thermogravimetric analysis of walnut shell as pyrolysis feedstock, J. Therm. Anal. Calorim. 105 (1) (Jul. 2011) 145–150, https://doi.org/10.1007/s10973-010-1267-x.

[52] A.R. Albis Arrieta, E. Ortiz Muñoz, I. Piñeres Ariza, A.F. Suárez Escobar, M.C. Vanegas Chamorro, Devolatilization of african palm (elaeis guineensis) husk studied by TG-MS, Ing. Invest. 38 (2) (May 2018) 9–17, https://doi.org/10.15446/ing.investig.v38n2.67743.

[53] L. Basile, A. Tugnoli, V. Cozzani, Influence of macrocomponents on the pyrolysis heat demand of lignocellulosic biomass, Ind. Eng. Chem. Res. 56 (22) (Jun. 2017) 6432–6440, https://doi.org/10.1021/acs.iecr.7b00559.

[54] A.R. Albis, E.O. Munoz, I.P. Ariza, A.F. Suarez Escobar, C.S. Ariza Barraza, TG characterization of pyrolysis of cassava starch residues catalyzed by ferric sulfate, Contemporary Engineering Sciences 11 (72) (2018) 3587–3597, https://doi.org/10.12988/ces.2018.87365.

[55] B. Igliński, W. Kujawski, U. Kiełkowska, Pyrolysis of waste biomass: technical and process achievements, and future development—a review, Energies 16 (4) (Feb. 2023) 1829, https://doi.org/10.3390/en16041829.

[56] J.J.M. Orfão, F.J.A. Antunes, J.L. Figueiredo, Pyrolysis kinetics of lignocellulosic materials—three independent reactions model, Fuel 78 (3) (Feb. 1999) 349–358, https://doi.org/10.1016/S0016-2361(98)00156-2.

[57] J. Cai, L. Ji, Pattern search method for determination of DAEM kinetic parameters from nonisothermal TGA data of biomass, J. Math. Chem. 42 (3) (Aug. 2007) 547–553, https://doi.org/10.1007/s10910-006-9130-9.

[58] H. Yang, R. Yan, H. Chen, D.H. Lee, C. Zheng, Characteristics of hemicellulose, cellulose and lignin pyrolysis, Fuel 86 (12–13) (Aug. 2007) 1781–1788, https://doi.org/10.1016/j.fuel.2006.12.013.

[59] A. Meng, H. Zhou, L. Qin, Y. Zhang, Q. Li, Quantitative and kinetic TG-FTIR investigation on three kinds of biomass pyrolysis, J. Anal. Appl. Pyrolysis 104 (Nov. 2013) 28–37, https://doi.org/10.1016/J.JAAP.2013.09.013.

[60] X. Zhou, W. Li, R. Mabon, L.J. Broadbelt, A critical review on hemicellulose pyrolysis, Energy Technol. 5 (1) (Jan. 2017) 52–79, https://doi.org/10.1002/ente.201600327.